Revision 1.

Ryabchikovite, $CuMg(Si_2O_6)$, a new pyroxene group mineral, and some genetic features of natural anhydrous copper silicates

Nadezhda V. Shchipalkina[1]*, Oleg S. Vereshchagin[2], Igor V. Pekov[1,3], Dmitry I. Belakovskiy[4], Natalia N. Koshlyakova[1], Vladimir V. Shilovskikh[5], Dmitriy V. Pankin[6], Sergey N. Britvin[2], Fedor D. Sandalov[1], Evgeny G. Sidorov[7†]

[1]Faculty of Geology, Moscow State University, Vorobievy Gory, Moscow, 119991, Russia
[2]Institute of Earth Sciences, St Petersburg State University, University Embankment 7/9, St. Petersburg, 199034, Russia
[3]Vernadsky Institute of Geochemistry and Analytical Chemistry, Russian Academy of Sciences, Kosygina str. 19, Moscow, 119991, Russia
[4]Fersman Mineralogical Museum of the Russian Academy of Sciences, Leninsky Prospekt 18-2, Moscow, 119071, Russia
[5]Geomodel Resource Centre, St. Petersburg State University, Uliyanovskaya St. 1, St. Petersburg, 198504, Russia
[6]Center for Optical and Laser Materials Research, St. Petersburg State University, Uliyanovskaya St. 5, St. Petersburg, 198504, Russia
[7]Institute of Volcanology and Seismology, Far Eastern Branch of Russian Academy of Sciences, Piip Boulevard 9, Petropavlovsk-Kamchatsky, 683006, Russia
*E-mail: estel58@yandex.ru

† Deceased 20 March 2021

Abstract. Ryabchikovite, ideally $CuMg(Si_2O_6)$, a new pyroxene-group mineral (IMA No. 2021-011) was discovered in exhalations of the active Arsenatnaya fumarole, Tolbachik volcano, Kamchatka, Russia. The associated minerals are diopside, hematite, cuprospinel, fluorophlogopite, anhydrite, johillerite, tilasite and aphthitalite-group sulfates. Ryabchikovite forms thin (up to 25 μm) light brown to reddish-brown epitactic crusts on short-prismatic brownish-grey crystals of diopside (up to 0.5 mm). The new mineral is optically biaxial (+), $\alpha = 1.685(5)$, $\beta = 1.690(5)$, $\gamma = 1.703(4)$, and $2V$ (meas.) = 60(15)°. The average chemical composition (wt.%, electron microprobe data) is: MgO 18.05, CaO 0.77, CuO 26.46, ZnO 2.23, Al_2O_3 0.93, Fe_2O_3 1.89, SiO_2 50.10, total 100.43. The empirical formula calculated based on 6 O atoms per formulae unit is $(Mg_{1.05}Cu_{0.78}Zn_{0.06}Fe^{3+}_{0.06}Ca_{0.03})(Si_{1.96}Al_{0.04}O_6)$. Electron backscattered diffraction and powder X-

ray diffraction data show that ryabchikovite is a Cu,Mg-ordered analogue of clinoenstatite. Ryabchikovite adopts the space group $P2_1/c$ and has the following unit-cell parameters: a = 9.731(9), b = 8.929(8), c = 5.221(4) Å, β = 110.00(6)°, V = 426.3(7) Å^3, and Z = 4. Ryabchikovite is named in honor of the outstanding Russian geochemist and petrologist Igor Dmitrievich Ryabchikov (1937–2017). Our studies reveal that copper analogues of rock-forming minerals could be found in fumarolic system. Their crystallization does not require high temperatures or / and pressures (below 500 ºC / Pa).

Keywords: ryabchikovite, new mineral, pyroxene, fumarole sublimate, copper silicate, gas transport reaction, Tolbachik volcano

Introduction

The pyroxene group minerals are among the most widespread and well-studied. The main results of long-time period research of different characteristics of pyroxenes (chemical variability, crystal chemistry, spectroscopy, thermodynamics and applications) were summarized by Prewitt (1980). The general formula of pyroxenes is $M2M1(T_2O_6)$ (Morimoto et al. 1988). The species-defining components in earlier known natural pyroxenes are as follows: $M1$ = Mn^{2+}, Fe^{2+}, Mg^{2+}, Zn^{2+}, Sc^{3+}, Ti^{3+}, V^{3+}, Cr^{3+}, Mn^{3+}, Fe^{3+}, Al, $M2$ = Mg^{2+}, Fe^{2+}, Mn^{2+}, Li, Ca, Na, and T = Si, Al (International Mineralogical Association List of Minerals, www.ima-mineralogy.org). The detailed description of structural variations in pyroxenes is given by Cameron and Papike (1981). Pyroxenes are polygenic minerals formed in different magmatic, metamorphic and metasomatic rocks, which can be used as markers of p-T conditions. Besides the usual for pyroxene-group minerals formation conditions, some pyroxenes (enstatite, clinoenstatite and diopside) were found in exhalations of active and extinct volcanic fumaroles (Getahun et al. 1996; Symonds et al., 1987; Tessalina et al. 2008; Naboko and Glavatskikh 1992).

The possible solid solutions in natural pyroxenes were discussed in detail by Peter Robinson in the corresponding chapter of the handbook (Prewitt 1980) and crystal chemical features were summarized by Morimoto (1989). Noteworthy, pyroxenes with the distinct Cu content (> 1 wt.% CuO) had not been found in nature until our work on silicate mineralization from fumaroles of the Tolbachik volcano. Some samples of pyroxenes (diopside and enstatite) of fumarolic genesis, originating from the active Arsenatnaya fumarole (Tolbachik volcano, Kamchatka, Russia) contain up to 1.2 wt.% CuO (Shchipalkina et al. 2020). The origin of these pyroxenes is related to two processes: metasomatic alteration of host rocks by hot gas and primary crystallization from the gas. Pyroxenes of the diopside-aegirine-esseneite solid-solution system are of the main minerals in deep, hottest zones of the mentioned fumarole (Pekov et al. 2018a,

2020; Shchipalkina et al. 2020). Another location in which Cu impurity was detected in pyroxenes in minor amount (up to 120 ppm), is igneous rocks of Bingham – Park City Belt (Core et al. 2005). The issues of Cu incorporation into pyroxene crystal structure and its diffusion in natural pyroxenes were studied experimentally by Audetat et al. (2018). The maximum content of Cu on the surface of synthetic pyroxene samples obtained from these experiments is 427 ppm. Noteworthy the experiments were provided in a gas mixing furnace.

In this paper we describe the first natural pyroxene with species-defining copper, a new mineral species ryabchikovite, ideally $CuMg(Si_2O_6)$, from the exhalations of the Arsenatnaya fumarole and discuss processes of formation of this novel pyroxene. The mineral name is given in honor of the outstanding Russian geochemist and petrologist Professor Igor Dmitrievich Ryabchikov (1937–2017), Academician of the Russian Academy of Sciences who worked in the Institute of Geology of Ore Deposits, Petrography, Mineralogy and Geochemistry of the Russian Academy of Sciences (IGEM RAS), Moscow. Professor Ryabchikov made a great contribution to the thermodynamics of fluid phase in magmatic systems, to the knowledge on the distribution of rare elements in magmatic rocks, to the geochemistry and systematics of basaltoid and alkaline rocks and the geochemistry of mantle rocks.

Both the new mineral and its name have been approved by the IMA Commission on New Minerals, Nomenclature and Classification (IMA No. 2021-011). The type specimen is deposited in the systematic collection of the Fersman Mineralogical Museum of the Russian Academy of Sciences, Moscow under the catalogue number 97512.

Occurrence and general appearance of ryabchikovite

Ryabchikovite occurs at the Arsenatnaya fumarole located at the summit of the Second scoria cone of the Northern Breakthrough of the Great Tolbachik Fissure Eruption, Tolbachik volcano, Kamchatka peninsula, Far-Eastern Region, Russia, 55°41′N, 160°14′E, 1200 meters above sea level. This active oxidizing-type fumarole is characterized by outstanding mineral diversity. The mineralogy and zonation of the Arsenatnaya fumarole were described by us in detail (Pekov et al. 2018a; Shchipalkina et al. 2020).

Ryabchikovite was found in a single specimen collected in July 2015. Associated minerals are diopside, hematite, cuprospinel, fluorophlogopite, anhydrite, johillerite, tilasite and aphthitalite-group K-Na sulfates; secondary, supergene minerals closely associated with ryabchikovite are syngenite and hydroglauberite.

Ryabchikovite forms thin (up to 25 μm, typically no more than 10 μm) epitactic crusts on well-shaped short-prismatic to equant brownish-grey crystals of diopside (Figures 1 and 2) up to

0.5 mm in size. The surface of ryabchikovite crusts is rough (Figures 1 and 2). Diopside crystals with ryabchikovite crusts and hematite overgrow basalt scoria partially altered by fumarolic gas.

The temperatures 370–400°C were measured by us using chromel-alumel thermocouple in this area during the collecting. Ryabchikovite is a fumarolic mineral formed at temperatures not lower than 400–450ºC. We believe it was formed as a result of the interaction between Cu-bearing fumarolic gas and earlier formed diopside (for details see below).

Methods and results

Optical properties

Observation in plane polarized light shows ryabchikovite forms rims up to 10 micron epitactically overgrowing diopside crystals. Both are colorless, nonpleochroic. The refrative indexes were measured using Cargille immersion oils which were checked by refractometer before and after the measurements. Orientation of the grains was controled by conoscopical interferention figures. The estimation of the 2V angle for vatrix diopside was obtained from the curviness of the conoscopical figure on the section perpendicular to an optical axes. Ryabchikovite is optically biaxial (+), with $\alpha = 1.685(5)$, $\beta = 1.690(5)$, $\gamma = 1.703(4)$ (589 nm), $2V$ (meas.) = 60(15)°, and $2V$ (calc.) = 64°. Dispersion of optical axes was none observed. Orientation: $Z \wedge c = 47°$ (the c direction is considered to be parallel to the c direction of diopside crystal on which ryabchikovite forms parallel overgrowths). Optical properties of ryabchikovite are typical for monoclinic pyroxenes.

The observation under the microscope in plane polarized transmitted light, as well as the scanning electron images (Fig. 3), clearly shows that ryabchikovite forms parallel overgrowths on diopside. These minerals are similar but not identical in optical characteristics. They distinctly differ from one another in refractive indices. Diopside underlying ryabchikovite is optically biaxial (+), with $\alpha = 1.668(2)$, $\beta = 1.675(3)$, $\gamma = 1.691(2)$, and $2V$ (meas.) = 60(10)°. Their optical orientation is also different: $Z \wedge c = 42°$ for diopside and $Z \wedge c = 47°$ for the ryabchikovite crust.

Chemical composition

The chemical composition of ryabchikovite was studied using electron microprobe. The analyses were carried out with a JEOL JXA-8230 (WDS mode) at the Laboratory of Analytical Techniques of High Spatial Resolution, Dept. of Petrology, Moscow State University. The operating conditions included an accelerating voltage of 20 kV and beam current of 20 nA, beam was rastered on an area 4 μm × 4 μm. The data reduction was carried out by means of an INCA Energy 300 software package. The following standards were used for quantitative analysis: diopside (Mg), metal Cu (Cu), ZnS (Zn), anorthite (Ca, Al and Si), and metal Fe (Fe). Contents of other elements with atomic numbers higher than carbon are below detection limits. EDS maps

were obtained on a Hitachi S-3400N scanning electron microscope equipped with AzTec Energy X-Max 20 EDS under 20 kV accelerating voltage, 1.5 nA beam current, 60 sec dwell time. All the calculations and corrections were conducted automatically with Oxford AzTec software.

The analyses in Table 1 are arranged in the order of increasing CuO content. The empirical formula of ryabchikovite with maximum content of Cu (27.79 wt.%) based on 6 O atoms per formula unit (*apfu*) is $(Mg_{1.03}Cu_{0.85}Zn_{0.05}Ca_{0.04}Fe^{3+}_{0.03})_{\Sigma 2.00}Si_{1.99}O_6$. The average chemical composition (wt.%, electron microprobe data, ranges are in parentheses) is: MgO 18.05 (16.28 – 20.76), CaO 0.77 (0.00 – 1.21), CuO 26.46 (25.72 – 27.79), ZnO 2.23 (1.01 – 3.23), Al_2O_3 0.93 (0.88 – 0.99), Fe_2O_3 1.89 (0.99 – 3.07), SiO_2 50.10 49.00 – 52.62, total 100.43. The empirical formula is $(Mg_{1.05}Cu_{0.78}Zn_{0.06}Fe^{3+}_{0.06}Ca_{0.03})(Si_{1.96}Al_{0.04}O_6)$

Raman spectroscopy

The Raman spectrum of ryabchikovite (Fig. 3a) was obtained at LabRam HR800 (Horiba Jobin-Yvon) confocal Raman spectrometer using He-Ne laser (wavelength 632.8 nm) at Center for Optical and Laser Materials Research, St. Petersburg State University. The laser power under the 50x objective [N.A. (Numerical aperture) = 0.75] was 1 mW. The spectrum was recorded in the range of 50–4000 cm^{-1} with a resolution of 2 cm^{-1} and acquisition time 90 s with 5 repetitions. The spectrometer was calibrated using silicon standard peak at 520.7 cm^{-1}. The diameter of the laser spot on the sample was about 6 μm. The Raman spectra of well-studied enstatite, clinoenstatite and green and yellow diopside, all from the Arsenatnaya fumarole, are used for comparison. These spectra were recorded at an EnSpectr R532 spectrometer with a solid green laser (532 nm) at Dept. of Mineralogy, Moscow State University. The laser output power was about 7 mW. The spectrum was processed using the EnSpectr expert mode program in the range of 100-4000 cm^{-1} with the use of a holographic diffraction grating with 1800 lines/mm and a resolution equals to about 6 cm^{-1}. The diameter of the laser spot on the sample was about 10 μm. All spectra were obtained at room temperature and demonstrated at Fig. 3.

The Raman spectra of different orthorhombic and monoclinic pyroxenes are studied quite well (White 1975; Ohashi and Sekita 1982, 1983; Sekita et al. 1988; Ghose et al. 1994; Huang et al. 2000; Wang et al. 2001; Prencipe et al., 2012; Tribaudino et al. 2012, 2019 and references therein). Wang et al. (2001) distinguished five Raman frequency regions for pyroxenes: 1100–800 (I), 800–600 (II), 600–450 (III), 450–300 (IV), and below 300 cm^{-1} (V). The most characteristic region for identification of the monoclinic pyroxenes with the $P2_1/c$ and $C2/c$ space groups is 800–600 cm^{-1}. In pyroxenes with the $C2/c$ symmetry (e.g., diopside), there are symmetrically equivalent chains of tetrahedra, thus there is one strong band near 670 cm^{-1}, corresponding to the *Ag* symmetric stretching vibrations of Si-O_b-Si bonds in tetrahedral chains. In monoclinic pyroxenes

with $P2_1/c$ symmetry (e.g., clinoenstatite) and orthorhombic pyroxenes with *Pbca* symmetry (e.g., enstatite), this band is split due to the presence of two symmetrically independent chains (SiA and SiB) with different deformation angles. This «rule» is revealed clearly at the Raman spectra of clinoenstatite, enstatite and different crystals of diopside (Figs. 3b-e). In the region 1100-800 cm^{-1}, both enstatite and clinoenstatite may show a doublet (~1010 and ~1030 cm^{-1}) (Wang et al. 2001).

The set of bands and their frequencies in the Raman spectrum of ryabchikovite correspond to the spectra of clinopyroxenes (Figs. 3, 4). The spectrum of ryabchikovite contains broad and asymmetric bands in the regions 600–800 and 800–1100 cm^{-1}. This can be interpreted as pairs of poor resolved bands with maxima at 678 and at 998 cm^{-1} and a shoulder bands at 692 and 1014 cm^{-1}, respectively. Both doublets are inherent to the monoclinic pyroxenes with $P2_1/c$ symmetry, e.g. clinoenstatite (Fig. 3b). The Raman spectrum of ryabchikovite distinctly differs from the spectra of Cu-free pyroxenes – enstatite, clinoenstatite and diopside in the presence of intense band at 457 cm^{-1}. This band is assigned to stretching vibrations of the Cu^{2+}–O bond with length between 1.9 and 2.0 Å according to the results on synthetic analogue of this mineral (Ding et al. 2016). The bands corresponding to Cu^{2+}–O stretching vibrations in the range 440–460 cm^{-1} are present in Raman and infrared (IR) spectra of some natural and synthetic copper compounds with Cu^{2+}-centered polyhedra characterized by the strong Jahn-Teller distortion which demonstrate short Cu^{2+}–O distances, 1.85–2.0 Å. It was reported, e.g., for the Raman spectra of ericlaxmanite and kozyrevskite, two polymorphs of $Cu_4O(AsO_4)_2$ (Pekov et al. 2014), and discussed for the IR spectra of synthetic analogue of yaroshevskite $Cu_9O_2(VO_4)_4Cl_2$ and related compounds (Siidra et al. 2020). The presence of strong band at 456 cm^{-1} is an evidence of the polyhedron with the strong Jahn-Teller distortion in ryabchikovite as a result of the significant Cu-Mg ordering in its structure. The absence of functional groups with O-H, C-H, N-H, B-O confirmed by absence of Raman-active stretching vibration peaks in the region higher than 1100 cm^{-1}.

Electron backscatter diffraction (EBSD)

The samples were polished with progressively smaller polycrystalline diamond suspensions with the ending step of Ar ion etching for 10 min at the final stage (Oxford IonFab 300) to remove the amorphized layer for electron backscatter diffraction (EBSD) analysis. EBSD measurements of ryabchikovite were carried out by means of a Hitachi S-3400N scanning electron microscope equipped with an Oxford Instruments Nordlys-HKL EBSD detector, operated at 20 kV and 1.5 nA in a focused beam mode, using a 70° tilted stage. EBSD mapping was performed with 2 × 2 binning and no averaging, final exposition was 40 msec per point. Both acquisition and analysis of Kikuchi patterns were performed using Oxford AZtecHKL software. EBSD orientation maps are presented as color-coded images using standard techniques of color-coded visualization

of Euler angles (Fig. 5). Phase maps are presented as color-coded images. The structures of the phases were determined by matching the respective EBSD patterns with the reference structural models obtained from Inorganic Crystal Structure Database (ICSD).

Structural identification was carried out by matching the obtained EBSD patterns with the reference structure of monoclinic $^{M2}Cu_{0.8}{}^{M1}Mg_{1.2}(Si_2O_6)$ (space group $P2_1/c$ and unit-cell parameters: a = 9.7352 Å, b = 8.9020, c = 5.2268 Å, β = 110.72°, V = 423.66 Å^3, and Z = 4) (Ding et al. 2016). The best attained mean angular deviation (MAD) is 0.36° for 12 Kikuchi bands (Fig. 6). Fitting of the EBSD patterns for an orthorhombic $^{M2}(Cu_{0.56}Mg_{0.44})^{M1}Mg(Si_2O_6)$ model (sp. gr. Pbca) (Tachi et al. 1997) resulted in the parameter MAD = 0.64° for only 8 Kikuchi bands. Moreover, the obtained solution does not describe a number of existing intensive bands. Thus, the orthorhombic model is not suitable for ryabchikovite.

Powder X-ray diffraction (PXRD) data

PXRD data for ryabchikovite (intergrowth with diopside) were collected using a Rigaku R-AXIS Rapid II diffractometer (image plate), Co$K\alpha$, 40 kV, 15 mA, rotating anode with the microfocus optics, Debye-Scherrer geometry, d = 127.4 mm, exposure 15 min. The data were processed using the osc2xrd program (Britvin et al. 2017) and Stoe WinXPOW software (Stoe and Cie 2006). Data (in Å for Co$K\alpha$ radiation) are listed in Table 2. Unit-cell parameters of monoclinic unit cell (sp.gr. $P2_1/c$) of ryabchikovite refined from the powder data are as follows: (sp.gr. $P2_1/c$) a = 9.731(9), b = 8.929(8) Å, c = 5.221(4) Å, β = 110.00(6)°, V = 426.3(7) Å^3, Z = 4.

Discussion

Crystal chemistry of Cu-bearing pyroxenes

The interest to the pyroxenes with so-called "Jahn-Teller cations", such as Co^{2+}, Cu^{2+} and Cr^{2+}, does not fade. These cations tend to have the square planar coordination by oxygen atoms. Data on the pyroxenes with different divalent cations were summarized by Cameron and Papike (1981) and Morimoto (1989). However, the pyroxenes with "Jahn-Teller cations" were known to date only as synthetic compounds.

The study of synthetic Cu-bearing pyroxene analogues with (Si_2O_6) and (Ge_2O_6) was started from 1960s (Borchert and Krämer, 1969). The data on synthetic Cu-rich silicate pyroxene analogues are summarized in Table 3. The first successful synthesis of $CuMg(Si_2O_6)$ with low-clinopyroxene crystal structure ($P2_1/c$) was done by Breuer et al. (1986). The crystal structure of this compound, including distribution of Cu and Mg among the *M2* and *M1* sites, were obtained

from the PXRD data. The Cu^{2+} and Mg cations were considered being ordered at *M*2 and *M*1 sites, respectively. The preference of Cu^{2+} to the *M*2 site in pyroxene-type structure was also shown by Ghose and Wan (1976) and Tachi et al. (1997) for Cu-bearing orthopyroxenes with the space group *Pbca*. The arrangement of O atoms around the Cu^{2+} site in this compound is close to the distorted square pyramidal with five-fold coordination, but non to the square planar shape expected from the Jahn-Teller effect (Tachi et al. 1997). The recent research of Cu-bearing clinopyroxene was undertaken by Ding et al. (2016) who synthesized $Cu_{0.8}Mg_{1.2}Si_2O_6$ from Cu^{2+} acetate and Mg acetate with calcination at t = 1000°C during 10 hours. According to the Rietveld refinement, this compound belongs to the low-clinopyroxene structure type ($P2_1/c$). The Cu^{2+} and Mg cations are ordered despite their close ionic radii (0.73 and 0.72 Å, respectively, Shannon, 1976): Mg occupies the *M*1 site whereas Cu^{2+} and residual Mg are localized at the *M*2 site. The *M*2 polyhedron is the octahedron strongly distorted due to the Jahn-Teller effect: Cu–O distances vary from 1.81 to 2.76 Å (Ding et al. 2016); it could be reduced to the five-fold polyhedron with Cu–O distances from 1.81 to 2.38 Å. Noteworthy, that $CaCuSi_2O_6$ with pyroxene structure has not been synthesized yet despite many attempts.

Ryabchikovite, the first copper-rich natural pyroxene, is considered as a natural analogue of synthetic monoclinic ($P2_1/c$) pyroxene with the ideal formula $CuMg(Si_2O_6)$ reported by Breuer et al. (1986) and Ding et al. (2016). The monoclinic crystal system and the space group $P2_1/c$ of ryabchikovite is typical for so-called low clinopyroxenes and undoubtedly confirmed by the combination of EBSD, PXRD, Raman spectroscopic and optical data. The predominance of Cu at the *M*2 and Mg at *M*1 in this pyroxene is considered based on the crystal chemical data on synthetic pyroxenes with Cu^{2+} and other "Jahn-Teller cations" (see references above). The presence of band at 456 cm^{-1} in the Raman spectrum of ryabchikovite (which is absent in the spectra of Cu-free pyroxenes) is another evidence of the significant Cu-Mg ordering: this demonstrates the presence of the polyhedron strongly distorted from the Jahn-Teller effect that is possible only as a result of its occupancy mainly with Cu^{2+}. The comparative data for studied pyroxenes from the exhalations of the Arsenatnaya fumarole are given in Table 4.

Formation conditions of Cu-rich anhydrous silicates

Copper is among rare elements in upper continental crust of the Earth, its content (28 μg/g) is the same as that of Nd (27 μg/g) or Ce (31 μg/g) (Rudnick and Gao 2003). However, more than 700 minerals with species-defining Cu are known (40 of with are copper silicates), whereas only 44 minerals with species-defining Nd were found up to date (and only 9 are neodymium silicates). Among minerals, the silicates with species-defining copper are not common and generally occur

in the oxidation zone of ore deposits. Most of copper silicates are hydrous. Eight H-free natural Cu silicates were described until recently, namely scottyite $BaCu_2(Si_2O_7)$ (Hentschel et al. 1993; Yang et al. 2013), effenbergerite $BaCu(Si_4O_{10})$ (Giester and Rieck 1994), cuprorivaite $CaCu(Si_4O_{10})$ (Minguzzi 1938; Mazzi and Pabst 1962), wesselsite $SrCu(Si_4O_{10})$ (Giester and Rieck 1996), colinowensite $BaCu(Si_2O_6)$ (Rieck et al. 2015), litidionite $CuNaK(Si_4O_{10})$ (Pozas et al. 1975), liebauite $Ca_3Cu_5(Si_9O_{26})$ (Zöller et al. 1992), and stavelotite-(La) $(La,Nd,Ca)_3Mn^{2+}{}_3Cu(Mn^{3+},Fe^{3+},Mn^{4+})_{26}(Si_2O_7)_6O_{30}$ (Bernhardt et al. 2005). Among these minerals, four species are known in high-temperature post-volcanic mineral associations formed with a participation of fumarolic gas: cuprorivaite, liebauite, litidionite, and scottyite-(La).

The Cu-bearing synthetic analogues are known for such rock-forming silicates as olivines, garnets, pyroxenes (Hrichova 1970; Breuer et al. 1986; Zabdyr and Fabrichnaya 2004; Tachi et al. 1997; Ding et al. 2016; Elthohamy et al. 2021). All mentioned silicates were synthesized in systems with high oxygen fugacity and atmospheric pressure by sintering of oxide mixtures, with or without flux. Finds of Cu-bearing micas and amphiboles in nature are known (Wang et al. 2019; Chukanov et al. 2020; Varlamov et al. 2021). Thus, the content of CuO in biotite from the Mulyashy copper mine (Zambia) is up to 6.0 wt.% and up to 1.4 wt.% in magnesio-riebeckite from metasomatic rocks of the Pelagonian Massif (Republic of North Macedonia), one of the rare example of sulfide-free endogenic ores with diverse oxygen-bearing minerals of Sb^{5+}, Zn, Pb and Cu. In the Pelagonian Massif, the total sulfur is precipitated in baryte, because of the great excess of Ba in the mineral-forming system (Chukanov et al. 2020). The Cu-bearing varieties of tourmalines (up to 3.6 wt.% CuO) (Vereshchagin et al. 2013) and vesuvianite-group mineral cyprine $Ca_{19}Cu^{2+}(Al,Mg,Mn)_{12}Si_{18}O_{69}(OH)_9$ (up to 2.5 wt.% CuO) (Panikorovskii et al. 2017) are also described and their origin is related to the hydrothermal/metasomatic processes. If we compare the *p-T-x* conditions of the geological settings with H_2O-free copper silicates, the following common features can be observed: high oxygen fugacity during the formation of silicates, the concentration of S in sulfates (no sulfides or only their relicts), low pressure (typically close to atmospheric one), the temperature of formation 500-1000°C The published data on partition coefficients of Cu (D_{Cu}) between silicate melts and crystalline silicates show that D_{Cu} (mineral/silicate melt) are as follows: for amphiboles – 0.06, olivines – 0.03-0.14, orthopyroxenes – 0.02-0.09 , clinopyroxenes – 0.02-0.23, garnets – 0.03-0.05 (Liu 2014; Roux et al. 2015; Hsu et al. 2017; Portnyagin et al. 2017 and references therein) and this value increases with increasing of fO_2. This seems to be important for the above-discussed geological settings.

It is known, that despite the strong enrichment of copper in usual volcanic settings no Cu-rich silicates were detected from the associations with Cu sulfides because of strong affinity of Cu to covalent bonding with sulfur in sulfidic form (chalcophile behavior). The distinctive feature of

the described fumarolic systems related to the Tolbachik volcano is strongly oxidizing conditions of mineral formation. This is a result of the mixing of hot volcanic gas with atmospheric air. Some oxidizing-type fumaroles related to Tolbachik are strongly enriched with copper and thus a uniquely abundant and diverse Cu^{2+} mineralization forms there at temperatures 300-600°C (Pekov et al. 2018b). The review on fumarolic copper mineralization presented by Pekov et al. (2018b) shows that Cu-rich minerals in the Tolbachik fumaroles (including Arsenatnaya) are mainly represented by various sulfates and arsenates, which demonstrate the zonal distribution in vertical section of fumaroles. In near-surface zones of the Arsenatnaya fumarole, the main sublimate copper minerals are sulfates – euchlorine $KNaCu_3O(SO_4)_3$, wulffite $K_3NaCu_4O_2(SO_4)_4$, chalcocyanite $CuSO_4$, dolerophanite $Cu_2O(SO_4)$, and fedotovite $K_2Cu_3O(SO_4)_3$. The Cu-rich mineralization is traced up to the 1.5 meter depth. The deepest Cu-rich zone is enriched by arsenates among which the Cu^{2+} arsenates dominate, mainly johillerite $NaCuMg_3(AsO_4)$, bradaczekite $NaCu_4(AsO_4)_3$, and lammerite $Cu_3[(As,P)O_4]_2$. Litidionite and ryabchikovite were found especially in this zone, as well as yangzhumingite $KMg_{2.5}(Si_4O_{10})F_2$ with 1.4 wt.% of CuO and potassic-magnesio-fluoro-arfvedsonite $KNa_2(Mg_4Fe^{3+})(Si_8O_{22})F_2$ with 1.7 wt.% of CuO (Shchipalkina et al. 2020). Below this zone, the Cu-bearing minerals disappear. As our data show, silicates of deep zones contain no more than 0.5 wt.% CuO (e.g., forsterite). However, such Cu content is quite high for olivine of any other genesis and was not detected earlier in natural samples. For comparison, in fumaroles of the famous Vesuvius volcano (Campania, Italy) only two exhalation silicates are known, litidionite and cuprorivaite (Balassone et al. 2019). The mentioned copper silicates are rare in fumarolic assemblages at both volcanoes. Unfortunately, the poorly resolved issue for both described fumarolic localities is the staging of changes in gas composition conjugating with deposition of different mineral paragenesis, influence of dominating components in gas on gradual alteration of hosting rocks and redeposition of earlier formed minerals.

As aforementioned, ryabchikovite occurs as thin epitactic crusts on diopside crystals. The optical and EBSD data verified the orientations of diopside substrate and ryabchikovite crusts to be identical (Fig. 5). The character of some borders between diopside and ryabchikovite can be interpreted as a sign of the replacement of diopside by ryabchikovite (Figures 1 and 2). There is no intermediate transition zone in Ca, Mg and Cu contents between diopside and ryabchikovite in these intergrowths (Fig. 7). This is displayed on X-ray maps of Cu, Ca and Mg (Fig. 7). This can be an evidence of formation of ryabchikovite during the process of alteration of diopside by hot and chemically "aggressive" fumarolic gas probably strongly enriched with Cu under oxidizing conditions. Such process is indirectly confirmed by the presence of cuprospinel $CuFe^{3+}{}_2O_4$ crusts on hematite in the same sample with ryabchikovite crusts on diopside. The experiments on

synthesis of Cu-bearing pyroxenes described above show the formation of Cu-rich pyroxenes is possible from the melt enriched in Cu, solid state diffusion or vaporization of components with formation of precursor for crystallization copper silicates (Breuer et al. 1986; Ding et al. 2016). In our case, the most plausible way is the crystallization of ryabchikovite due to the precursor – the initial diopside, which was partly altered by gas containing, presumably, copper halide. The signs of local strongly enrichment in Cu, not bonded with any form of S, are the presence of Cu-bearing varieties of yangzhumingite and potassic-magnesio-fluoro-arfvedsonite in the same zone as ryabchikovite. These silicates are associated with members of the NaCl–KCl solid-solution series (so-called 'sylvinite'), which can indirectly indicate the transport of Cu in halide form during their crystallization. The possibility of formation of rims on diopside single crystal during the reaction with MCl_2 (where M = Ni, Mg), but in aqueous solutions at t = 300-600°C and p = 100 MPa was shown by Majumdar (2014). In these experiments the outer rim with the thickness 10 and 15 μm consists of willemseite $Ni_3Si_4O_{10}(OH)_2$.

Summarizing the discussion above, several factors can lead to the formation of H-free Cu-enriched silicates: high oxygen fugacity coupled with relatively low pressure (close to atmospheric one), presumably, halides as transport agents for Cu on the stage of silicate crystallization in post-volcanic systems, the sulfur fixed mainly in sulfate form, and local supersaturation in Cu during the deposition of silicates.

Implications Our studies reveal, that copper analogues of rock-forming minerals could be found in fumarolic system. Their crystallization does not require high temperatures or / and pressures (below 500 ºC / Pa), which was confirmed by studies of ryabchikovite $CuMg(Si_2O_6)$. We assume, that copper rich analogues of mica, tourmaline could be found in this systems. Besides, silicates with Jahn-Teller cations, in particular pyroxenes, are in the field of materials science interest as they possess multiferroic properties and quasi-one-dimensional magnetic behavior . Described origin of ryabchikovite, the first natural pyroxene with species-defining copper, shows that such pyroxenes can growth during the gas-transport reactions at relatively low temperatures at atmospheric pressure with diopside as a precursor. This can be useful for a development of chemical technologies based on gas-transport reaction for material science applications

Acknowledgements We are grateful to Mario Tribaudino, Frank C. Hawthorne and the anonymous reviewer for valuable comments and suggestions for improving the paper, and Fabrizio Nestola for his editorial work. This work was supported by the Russian Science Foundation, grant no. 19-17-00050. The authors thank the Resource Center of X-ray diffraction studies and Geomodel Resource Centre of Saint-Petersburg State University for providing instrumental and

computational resources. The Raman measurements has been partly performed at SPbSU Research park Center for optical and laser materials research with financial support from St. Petersburg State University (project No 93021679)

Declarations

Conflict of interest The authors have no competing interests to declare that are relevant to the content of this article.

Ethical approval Hereby, the authors consciously assure that following statements are fulfilled: 1. this manuscript is the authors' original work, which has not been previously published elsewhere. 2. This manuscript is not currently being reviewed for publications elsewhere. 3. This manuscript reflects the authors' own research and analysis in a truthful and complete manner. 4. This manuscript properly credits valuable contributions from co-authors. 5. All references are properly cited.

Consent to participate Hereby, the authors consciously assure that following statements are fulfilled: 1. All the authors have contributions to the current manuscript. 2. All the authors take public responsibilities to the current manuscript.

REFERENCES

Audetat, A., Zhang, L., and Huaiwei, N. (2018) Copper and Li diffusion in plagioclase, pyroxenes, olivine and apatite, and consequences for the composition of melt inclusions. Geochimica et Cosmochimica Acta, 243, 99-115.

Balassone, G., Petti, C., Mondillo, N., Panikorovskii, T.L., Gennao, R., Capelletti, P., Altomare, A., Corriero, N., Cangiano, M., and D'Orazio, L. (2019) Copper minerals at Vesuvius volcano (Southern Italy): a mineralogical review. Minerals, 9, Paper 730.

Bernhardt, H.J., Armbruster, T., Fransolet, A.M., and Schreyer, W. (2005) Stavelotite-(La), a new lanthanum-manganese-sorosilicate mineral from the Stavelot Massif, Belgium. European Journal of Mineralogy, 17, 703-714.

Borchert, W., and Krämer, V. (1969) Ein synthetisches Magnesium-Kupfer-Silikat mit Klinopyroxenstruktur, $(Mg,Cu)_2[Si_2O_6]$. Neues Jahrbuch für Mineralogie - Abhandlungen, 6-14.

Breuer, K-H., Eysel, W., and Behruzi, M., (1986) Copper(II) silicates and germanates with chain structures. II. Crystal chemistry. Zeitschrift für Kristallographie, 176, 219–232.

Britvin, S.N., Dolivo-Dobrovolsky, D.V., and Krzhizhanovskaya, M.G. (2017) Software for processing the X-ray powder diffraction data obtained from the curved image plate detector of Rigaku RAXIS Rapid II diffractometer. Zapiski RMO, 146(3), 104-107. (in Russian)

Cameron, M., and Papike, J.J. (1981) Structural and chemical variations in pyroxenes. American Mineralogist, 66, 1–50.

Chukanov, N.V., Zubkova, N.V., Jancev, S., Pekov, I.V., Ermolaeva, V.N., Varlamov, D.A., Belakovskiy, D., and Britvin, S.N. (2020) Zinc-rich and copper-bearing amphiboles from sulphide-free ore occurences of the Pelagonian Massif, Republic of North Macedonia. Mineralogy and Petrology, 114, 129-140.

Core, D.P., Kesler, S.E., Essene, E.J., Dufresne, E.B., Clarke, R., Arms, D.A., Walko, D., Rivers, M. (2005) Copper and zinc in silicate and oxide minerals in igneous rocks from the Bingham – Park City Belt, Utah: synchrotron X-ray fluorescence data. Canadian Mineralogist, 43, 1781-1796.

Ding, L., Darie, C., Colin, C.V., and Bordet, P. (2016) $Cu_{0.8}Mg_{1.2}Si_2O_6$: a copper-bearing silicate with the low-clinopyroxene structure. Mineralogical Magazine, 80(2), 325-335.

Eltohamy, M.R., Ali, A.F., Leonelli, C., and Namzawy, E.M.A. (2021) Synthesis of Cu-containing diopside through a one-step crystallization. Egypt Journal of Chemistry, 64(11), 6673-6679.

Getahun, A., Reed, M.H., and Symonds, R. (1996) Mount St. Augustine volcano fumarole wall rock alteration: mineralogy, zoning, composition and numerical models of its formation process. Journal of Volcanology and Geothermal Research, 71, 73-107.

Ghose, S., Choudhury, N., Chaplot, S.I., Pal Chowdhury, C., and Sharma, S.K. (1994) Lattice dynamics and Raman spectroscopy of protoenstatite $Mg_2Si_2O_6$. Physics and Chemistry of Minerals, 20, 469-477.

Ghose, S., and Wan, C. (1976) Site preference of Cu^{2+}-ions in enstatite and the refinement of the crystal structure of a pure enstatite. EOS, 57, 337

Giester, G., and Rieck, B. (1994) Effenbergite, BaCu[Si4O10], a new mineral from the Kalahari Manganese field, South Africa: description and crystal structure. Mineralogical Magazine, 58, 663-670.

Giester, G., and Rieck, B. (1996) Wesselsite, $SrCu[Si_4O_{10}]$, a further new gillespite-group mineral from the Kalahari Manganese Field, South Africa. Mineralogical Magazine, 60(5), 795-798.

Henley, R.W., and Berger, B.R. (2013) Nature's refineries – Metals and metalloids in arc volcanoes. Earth Science Reviews, 125, 146-170.

Hentschel, G. (1993) Die Lavaströme der Graulai: eine neue Fundstelle in der Westeifel. Lapis, 12(9), 11-23. (in German) [as Unnamed (Ba-Cu Silicate) identical with synthetic $BaCu_2Si_2O_7$]

Hrichova, R. (1970) Contributions to the synthesis of spessartine analogues. Mineralogical Magazine, 37, 289.

Hsu, Y.J., Zajacz, Z., Ulmer, P., and Heinrich, C.A. (2017) Copper partitioning between silicate melts and amphibole: experimental insight into magma evolution leading to porphyry copper ore formation. Chemical Geology, 448, 151-163.

Le Roux, V., Dasgupta, R., Lee, C.T. (2015) Recommended mineral-melt partition coefficients for FRTEs (Cu), Ga and Ge during mantle melting. American Mineralogist, 100, 2533-2544.

Liu, X., Xiong, X., Audetat, A., Li, Y., Song, M., Li, L., Sun, W., and Ding, X. (2014) Partitioning of copper between olivine, orthopyroxene, clinopyroxene, spinel, garnet and silicate melts at upper mantle conditions. Geochimica et Cosmochimica Acta, 125, 1-22.

Majumdar, A.S., King, H.E., John, T., Kusebauch, C., and Putnis, A. (2014) Pseudomorphic replacement of diopside during interaction with $(Ni,Mg)Cl_2$ aqueous solutions: implications for the Ni-enrichment mechanism in talc- and serpentinite-type phases. Chemical Geology, 380, 27-40.

Mazzi, F., Pabst, A. (1962) Reexamination of cuprorivaite. American Mineralogist, 47, 409-410.

Minguzzi, C. (1938) Cuprorivaite: un nuovo minerale. Periodico di Mineralogia, 333-345.

Morimoto, N. (1989) Nomenclature of pyroxenes. Mineralogical Journal of Japan, 14(5), 198-221.

Naboko, S.I., and Glavatskikh, S.F. (1992) Relikty posteruptivnoy aktivnosty na starykh konusakh Tolbachinskogo dola, Kamchatka. Vulkanology and Seismology, 5-6, 66-86 (In Russian)

Ohashi, Y., and Sekita, M. (1982) Raman spectroscopic study of the Si-O-Si stretching vibration in clinopyroxenes. Journal of Japanese Association Mineral Petrol Econ Geology, 78, 239-245.

Ohashi, Y., and Sekita, M. (1983) Raman spectroscopic study of clinopyroxenes in the join $CaScAlSiO_6$-$CaTiAl_2O_6$. Journal of Japanese Association of Mineralogy, Petrology Economical Geology, 78, 239-245.

Panikorovskii, T.L., Shilovskikh, V.V., Avdontseva, E.Y., Zolotarev, A.A., Pekov, I.V., Britvin, S.N., Halenius, U., and Krivovichev, S.V. (2017) Cyprine, $Ca_{19}Cu^{2+}$(Al, Mg,

478 $Mn)_{12}Si_{18}O_{69}(OH)_9$, a new vesuvianite-group mineral from the Wessels mine, South
479 Africa. European Journal of Mineralogy, 29, 295-306.

480 Pekov, I.V., Koshlyakova, N.N., Zubkova, N.V., Lykova, I.S., Britvin, S.N., Yapaskurt, V.O.,
481 Agakhanov, A.A., Shchipalkina, N.V., Turchkova, A.G., and Sidorov, E.G. (2018a)
482 Fumarolic arsenates – a special type of arsenic mineralization. European Journal of
483 Mineralogy, 30, 305-322.

484 Pekov, I.V., Agakhanov, A.A., Zubkova, N.V., Koshlyakova, N.N., Shchipalkina, N.V., Sandalov,
485 F.D., Yapaskurt, V.O., Turchkova, A.G., and Sidorov, E.G. (2020) Oxidizing-type
486 fumaroles of the Tolbachik volcano, a mineralogical and geochemical unique. Russian
487 Geology and Geophysics, 61, 675-688.

488 Pekov, I.V., Zubkova, N.V., and Pushcharovsky, D.Yu. (2018b) Copper minerals from volcanic
489 exhalations – a unique family of natural compounds: crystal chemical review. Acta
490 Crystallographica, B74, 502-518.

491 Pekov, I.V., Zubkova, N.V., Yapaskurt, V.O., Belakovskiy, D.I., Vigasina, M.F., Sidorov, E.G.,
492 and Pushcharovsky, D.Yu. (2014) New arsenate minerals from the Arsenatnaya fumarole,
493 Tolbachik volcano, Kamchatka, Russia. II. Ericlaxmanite and kozyrevskite, two natural
494 modifications of $Cu_4O(AsO_4)_2$. Mineralogical Magazine, 78(7), 1553-1569.

495 Portnyagin, M.V., Mironov, N.L., and Nazarova, D.P. (2017) Copper partitioning between olivine
496 and melt inclusions and its content in primitive island-arc magmas of Kamchatka.
497 Petrology, 25, 419-432.

498 Pozas, J.M.M., Rossi, G., and Tazzoli, V. (1975) Re-examination and crystal structure analysis of
499 litidionite. American Mineralogy, 60, 471-474.

500 Prencipe M., Mantovani L., Tribaudino M., Bersani D., and Lottici P.P. (2012) The Raman
501 spectrum of diopside: a comparison between ab initio calculated and experimentally
502 measured frequencies. European Journal of Mineralogy, 24, 457-464.

503 Prewitt, C.T. (ed) (1980) Reviews in mineralogy. Volume 7. Pyroxenes. Berlin, Boston De
504 Gruyter.

505 Rieck, B., Pristacz, H., Giester, G. (2015) Colinowensite, $BaCuSi_2O_6$, a new mineral from the
506 Kalahari Manganese Field, South Africa and new data on wesselsite, $SrCuSi_4O_{10}$.
507 Mineralogical Magazine, 79(7), 1769-1778.

508 Sekita, M., Ohashi, H., and Terada, S. (1988) Raman study of clinopyroxene in the system
509 $CaScAlSiO_6 – CaAl_2SiO_6$($CaScAlSiO_6$-$CaTiAl_2O_6$). Physics and Chemistry of Minerals,
510 15, 319-322.

511 Shannon, R.D. (1976) Revised effective ionic radii and systematic studies of interatomic distances
512 in halides and chalcogenides. Acta Crystallographica, A32, 751-767.

513 Shchipalkina, N.V., Pekov, I.V., Koshlyakova, N.N., Britvin, S.N., Zubkova, N.V., Varlamov,
514 D.A., and Sidorov, E.G. (2020) Unusual silicate mineralization from fumarolic sublimates
515 of the Tolbachik volcano, Kamchatka, Russia. Part I. Ino-, cyclo-, neso-, phyllosilicates.
516 European Journal of Mineralogy, 32, 101-119.

Siidra, O.I., Vladimirova, V.A., Tsirlin, A.A., and Chukanov, N.V. (2020) $Cu_9O_2(VO_4)_4Cl_2$, the first copper oxychloride vanadate: mineralogically inspired synthesis and magnetic behavior. Inorganic Chemistry, 59(4), 2136-2143.

Symonds, R.B., Rose, W.I., Reed, M.H., Lichte, F.E., and Finnegan, D.L. (1987) Volatilization, transport and sublimation of metallic and non-metallic elements in high temperature gases at Merapi Volcano, Indonesia. Geochimica et Cosmochimica Acta, 51, 2083-2101.

Tachi, T., Horiuchi, H., and Nagasawa, H. (1997) Structure of Cu-bearing orthopyroxene, $Mg(Cu_{0.56}Mg_{0.44})Si_2O_6$ and behavior of Cu^{2+} in the orthopyroxene structure. Physics and Chemistry of Minerals, 24, 463-476.

Tessalina, S.G., Yudovskaya, M.A., Chaplygin, I.V., Birck, J.L., and Capmas, F. (2008) Sources of unique rhenium enrichment in fumaroles and sulphides at Kudryavy volcano. Geochimica et Cosmochimica Acta, 72, 889-909.

Tribaudino, M., Mantovani, L., Bersani, D., and Lottici, P.P. (2012) Raman spectroscopy of $(Ca,Mg)MgSi_2O_6$ clinopyroxenes. American Mineralogist, 97, 1339-1347.

Tribaudino, M., Stangarone, C., Gori, C., Mantovani, L., Bersani, D., and Lottici, P.P. (2019) Experimental and calculated Raman spectra in Ca-Zn pyroxenes and a comparison between $(Ca_xM^{2+}_{1-x})M^{2+}Si_2O_6$ pyroxenes (M^{2+} = Mg, Co, Zn, Fe^{2+}). Physics and Chemistry of Minerals, 46, 827-837.

Varlamov, D.A., Ermolaeva, V.N., Chukanov, N.V., and Jancev, S. (2021) Mineralogy of copper in nonsilfide endogeneous Pb-Zn-Sb ores of the Pelagonian Massif, Republic of North Macedonia. Zapiski RMO, 4, 103-114 (in Russian)

Vereshchagin, O.S., Rozhdestvenskaya, I.V., Frank-Kamenetskaya, O.V., Zolotarev, A.A., and Mashkovtsev, R.I. (2013) Crystal chemistry of Cu-bearing tourmalines. American Mineralogist, 98, 1610-1616.

Wang, A., Jolliff, B.L., Haskin, L.A., Kuebler, K.E., and Viskupic, K.M. (2001) Characterization and comparison of structural and compositional features of planetary quadrilateral pyroxenes by Raman spectroscopy. American Mineralogist, 86, 790–806.

Wang, G., Yang, H., Liu, Y., Tong, L., and Auwalu, A. (2019) The alteration mechanism of copper-bearing biotite and leachable property of copper-bearing minerals in Mulyashy Copper Mine, Zambia. Scientific Reports, 9, Paper 15040.

White, W.B. (1975) Structural interpretation of lunar and terrestrial minerals by Raman spectroscopy. In C. Karr, Jr., Ed., Infrared and Raman Spectroscopy of Lunar and Terrestrial Minerals, p. 325–358. Academic Press, New York.

Yang, H., Downs, R.T., Evans, S.H., Pinch, W.W. (2013) Scottyite, the natural analog of synthetic $BaCu_2Si_2O_7$, a new mineral from the Wessels mine, Kalahari Manganese Fields, South Africa. American Mineralogist, 98(2-3), 478-484.

Zabdyr, L.A., Fabrichnaya, O.B. (2004) Phase equilibria in the Co-Cu-O-Si system. Comp Coupl Ph Diagr Thermochem, 28, 293-298.

Zöller, M.H., Tillmanns, E., and Hentschel, G. (1992) Liebauite, $Ca_3Cu_5Si_9O_{26}$, a new silicate mineral with 14er single chain. Zeitschrift für Kristallographieallogr, 200, 115-126.

Figure captions

Figure 1. Crystals of diopside covered by light brown to reddish-brown ryabchikovite (Ryb) crust, with hematite (Hem) and white acicular supergene hydroglauberite (a). Aggregates of diopside (Di) crystals with ryabchikovite crust (b and c, SEM photos, SE mode)

Figure 2. Diopside (Di) crystals with crust of ryabchikovite (Ryb) overgrowing hematite (Hem). Polished sections, SEM images, BSE mode

Figure 3. The Raman spectra of ryabchikovite (a), clinoenstatite (sp. gr. $P2_1/c$) (b), enstatite (*Pbca*) (c) and diopside ($C2/c$) (d and e), all from the Arsenatnaya fumarole

Figure 4. Fragments of the Raman spectrum of ryabchikovite with bands in the regions 500–800 and 930–1080 cm^{-1}.

Figure 5. EBSD maps of polished sample with ryabchikovite (Ryb), diopside (Di) and hematite (HEM) from the Arsenatnaya fumarole: (a) mineral distribution map, (b) orientation map, (c) diopside crystals orientation, (d) ryabchikovite crystals orientation.

Figure 6. Example of Electron Backscatter Diffraction (EBSD) pattern (a) indexation using theoretical Kikuchi pattern generated from (b) synthetic monoclinic pyroxene $Cu_{0.8}Mg_{1.2}Si_2O_6$ (Ding *et al*., 2016) and (c) synthetic orthorhombic pyroxene $(Cu_{0.56}Mg_{0.44})MgSi_2O_6$ (Tachi *et al*., 1997).

Figure 7. Elemental maps of diopside (Di) – ryabchikovite (Ryb) intergrowth : (a) Ca-Cu-Mg, (b) CuKα, (c) Ca Kα and (d) Mg Kα.

This is the peer-reviewed, final accepted version for American Mineralogist, published by the Mineralogical Society of America.
The published version is subject to change. Cite as Authors (Year) Title. American Mineralogist, in press.
DOI: https://doi.org/10.2138/am-2022-8620. http://www.minsocam.org/

`Table 1. Chemical composition of ryabchikovite

	1	2	3	4	5	6	7	8
	wt%							
MgO	23.90	23.55	18.05	18.61	16.28	20.76	17.62	16.96
CaO	0.20	0.11	0.83	0.48	0.48	0.00	1.21	0.90
CuO	19.52	20.45	24.43	25.72	26.09	26.29	26.41	27.79
ZnO	1.17	1.38	2.64	2.49	3.23	1.01	2.76	1.65
Al_2O_3	2.34	1.51	1.23	0.84	0.99	0.00	0.96	0.00
Fe_2O_3	3.13	1.49	3.84	1.90	3.07	0.99	2.47	1.02
SiO_2	49.89	51.55	48.44	49.65	49.05	52.62	50.18	49.00
Total	100.15	100.04	99.46	99.69	99.19	101.67	101.61	99.27
	formula coefficients calculated based on 6 O *apfu*							
Mg	1.35	1.32	1.07	1.09	0.97	1.18	1.02	1.03
Ca	0.01	0.00	0.04	0.02	0.02	-	0.05	0.04
Cu	0.56	0.58	0.73	0.76	0.79	0.75	0.78	0.85
Zn	0.03	0.04	0.08	0.07	0.10	0.03	0.08	0.05
Al	0.10	0.07	0.06	0.04	0.05	-	0.04	-
Fe^{3+}	0.09	0.04	0.11	0.06	0.09	0.03	0.07	0.03
Si	1.88	1.94	1.92	1.95	1.96	2.00	1.95	1.99
Total*	4.02	4.00	4.00	4.00	3.97	3.99	3.99	3.99

*Sum of all metals and Si.

This is the peer-reviewed, final accepted version for American Mineralogist, published by the Mineralogical Society of America.
The published version is subject to change. Cite as Authors (Year) Title. American Mineralogist, in press.
DOI: https://doi.org/10.2138/am-2022-8620. http://www.minsocam.org/

Table 2. Powder X-ray diffraction data (d in Å) for ryabchikovite in comparison with the calculated data for its synthetic analogue (Ding et al. 2016)

Ryabchikovite		Synthetic $Cu_{0.8}Mg_{1.2}Si_2O_6$ (Ding et al., 2016)				
I_{obs}	d_{obs}	I_{calc}	d_{calc}	h	k	l
12	9.03	12	9.106	1	0	0
11	4.549	20	4.553	2	0	0
38	**4.403**	66	4.444	0	1	1
27	4.307	6	4.285	1	1	-1
18	3.986	3	3.999	1	2	0
32	3.746	8	3.755	1	1	1
7	3.497	7	3.483	2	1	-1
27	3.291	32	3.291	1	2	-1
100	**3.177**	100	3.183	2	2	0
***81**	**2.953**	71	2.945	2	1	1
75	**2.876**	51	2.873	3	1	0
***55**	**2.565**	61	2.569	0	3	1
26	2.456	55	2.444	2	0	-2
7	2.424	1	2.412	1	3	1
*6	2.393	14	2.409	3	2	-1
*6	2.343	3	2.354	1	0	2
		8	2.335	2	3	-1
		4	2.226	0	4	0
26	2.215	9	2.222	0	2	2
		13	2.179	4	1	-1
*36	2.157	52	2.150	2	3	1
***53**	**2.134**	6	2.143	2	2	-2
		4	2.124	3	2	1
21	1.990	13	1.999	2	4	0
*21	1.969	7	1.960	1	4	1
*4	1.909	1	1.918	2	4	-1
		10	1.893	4	0	-2
*4	1.861	2	1.878	2	2	2
*8	1.835	1	1.844	1	3	2
*4	1.814	1	1.812	2	4	1
6	1.740	12	1.742	4	2	-2
		5	1.682	0	5	1
10	1.682	7	1.682	2	1	-3
		9	1.681	0	4	2
***71**	**1.625**	28	1.628	4	3	1
		17	1.622	1	2	-3
		2	1.617	1	4	2
*29	1.616	6	1.614	5	1	-2
		3	1.611	2	5	-1
*5	1.565	6	1.560	4	0	2
9	1.551	2	1.556	3	4	-2
		8	1.546	2	5	1
*17	1.489	17	1.484	0	6	0
		12	1.483	2	3	-3
*18	1.478	5	1.481	0	3	3
		5	1.472	4	2	2
		1	1.428	3	3	-3
*16	1.425	1	1.425	1	3	3
		3	1.422	5	3	1
		2	1.420	1	5	2
*6	1.391	3	1.395	4	5	-1
5	1.372	6	1.372	1	4	-3

The seven strongest reflections are marked in boldtype.

* Overlapped reflections of ryabchikovite and diopside. In the low-angle region (d > 2.4 Å), the majority of reflections of ryabchikovite and diopside, the minerals different in unit-cell dimensions (Table 4), are well-resolved, whereas in the region with d < 2.4 Å many reflections of these clinopyroxenes are overlapped. This prevents the Rietveld refinement of the crystal structure of ryabchikovite.

This is the peer-reviewed, final accepted version for American Mineralogist, published by the Mineralogical Society of America.
The published version is subject to change. Cite as Authors (Year) Title. American Mineralogist, in press.
DOI: https://doi.org/10.2138/am-2022-8620. http://www.minsocam.org/

642 Table 3. Comparative data on synthetic Cu-rich pyroxenes

Formula	**$CuMg(Si_2O_6)$**	**$Cu_{0.8}Mg_{1.2}(Si_2O_6)$**	**$(Cu_{0.56}Mg_{0.44})Mg(Si_2O_6)$**
Method of synthesis	heating of the mixtures of CuO and MgO at 1000°C in air during 2-4 weeks	calcination of Cu acetate and Mg acetate at *t* = 1000°C during 10 h	heating of oxide-flux mixture to 850°C, and then stepped cooling to room temperature
Method of crystal structure study	powder X-ray diffraction	powder X-ray diffraction	single-crystal X-ray diffraction
Crystal system Space group	Monoclinic $P2_1/c$	Monoclinic $P2_1/c$	Orthorhombic *Pbca*
a, Å	9.731	9.7352	18.221
b, Å	8.918	8.9019	8.890
c, Å	5.224	5.2267	5.2260
β, °	110.52	110.721	90
V, Å^3	424.6	423.67	846.53
Occupancy of cation sites			
*M*2	$Cu_{1.00}$	$Cu_{0.72}Mg_{0.28}$	$Cu_{0.5}Mg_{0.5}$
*M*1	$Mg_{1.00}$	$Mg_{0.93}Cu_{0.07}$	Mg
Reference	Breuer et al. 1986	Ding et al. 2016	Tachi et al. 1997

643
644
645
646

647 Table 4. Comparative data on ryabchikovite, clinoenstatite and diopside from the Arsenatnaya
648 fumarole, Tolbachik volcano

Mineral	**Ryabchikovite**	**Clinoenstatite**	**Diopside**
Ideal formula	$CuMg(Si_2O_6)$	$MgMg(Si_2O_6)$	$CaMg(Si_2O_6)$
Crystal system Space group	Monoclinic $P2_1/c$	Monoclinic $P2_1/c$	Monoclinic $C2/c$
a, Å	9.731(9)	9.66(6)	9.746(2)
b, Å	8.929(8)	8.89(4)	8.879(1)
c, Å	5.221(4)	5.22(3)	5.281(1)
β, °	110.00(6)	108.6(8)	105.91(1)
V, Å^3	426.3(7)	426(1)	439.6(1)
Z	4	4	4
D_{calc}, g cm^{-3}	3.68	3.18	3.34
Raman bands, cm^{-1}	74, 94,107, 153, 179, 226, 324, 378, 457, 519, 541, 562, 678, 692, 838, 873, 916, 998, 1014, 1090	238, 300, 342, 381, 401, 419, 445, 521, 544, 581, 663, 684, 753, 853, 928, 1011, 1030	324, 349, 384, 501, 531, 661 705, 765, 813, 1002, 1040, 1102
Source	This work	Shchipalkina et al. 2020; this work (in part of Raman spectra)	

649

This is the peer-reviewed, final accepted version for American Mineralogist, published by the Mineralogical Society of America.
The published version is subject to change. Cite as Authors (Year) Title. American Mineralogist, in press.
DOI: https://doi.org/10.2138/am-2022-8620. http://www.minsocam.org/

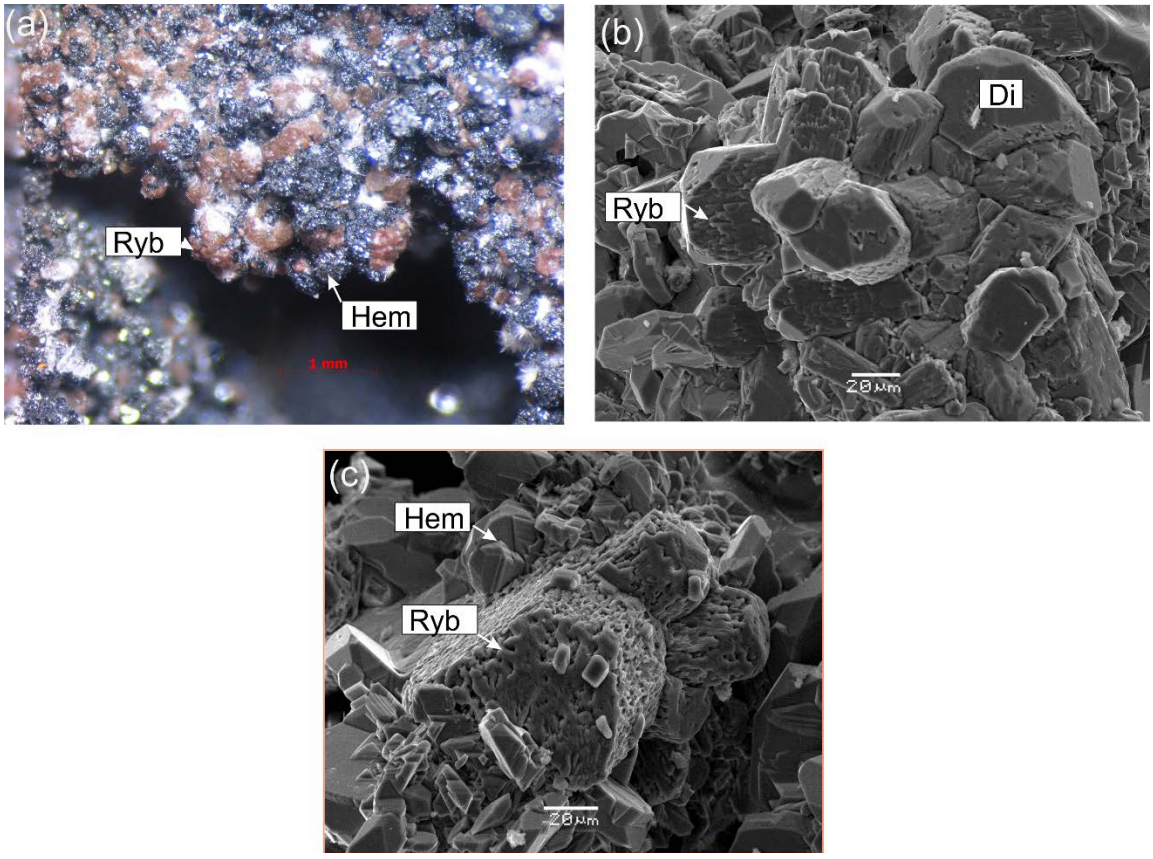

Figure 1. Crystals of diopside covered by light brown to reddish-brown ryabchikovite (Ryb) crust, with hematite (Hem) and white acicular supergene hydroglauberite (a). Aggregates of diopside (Di) crystals with ryabchikovite crust (b and c, SEM photos, SE mode)

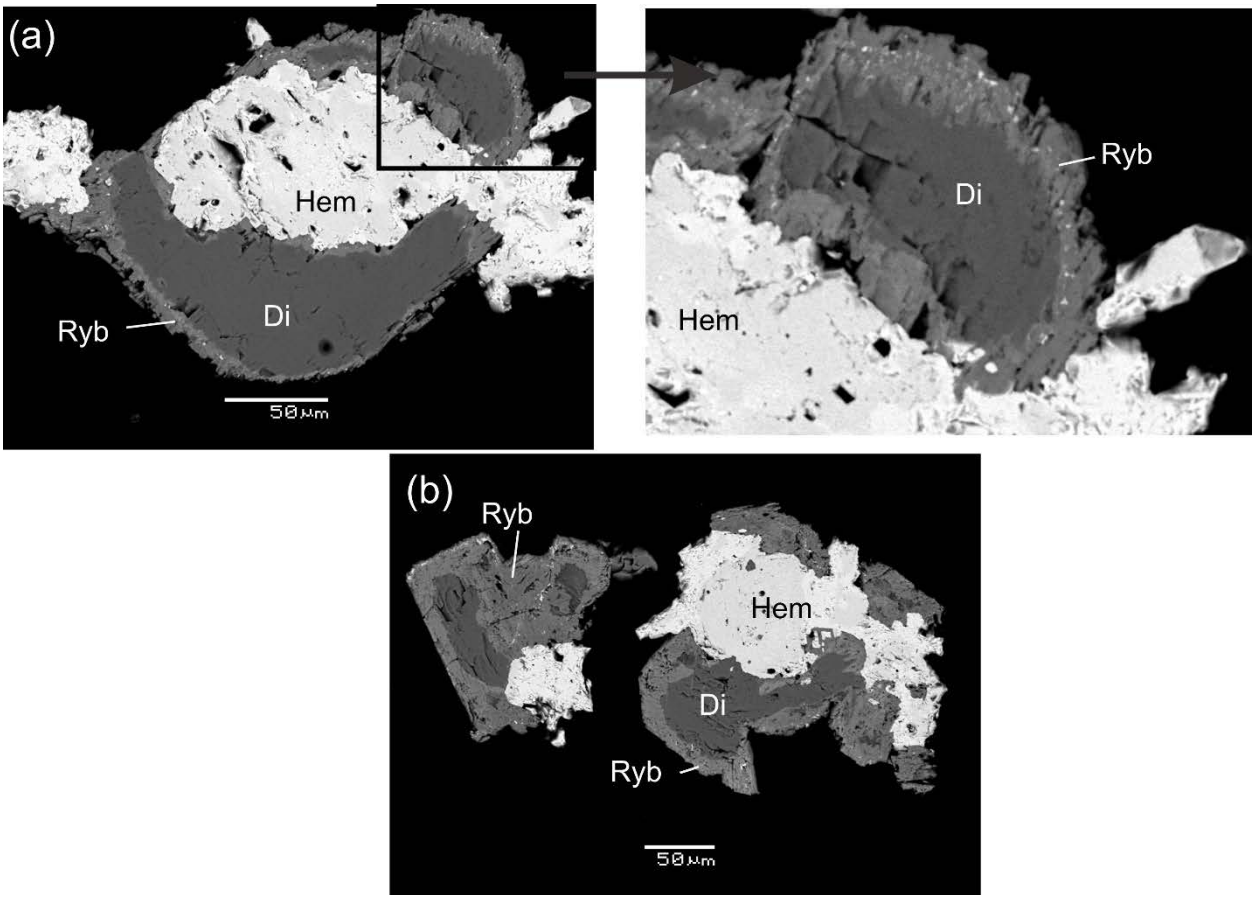

Figure 2. Diopside (Di) crystals with crust of ryabchikovite (Ryb) overgrowing hematite (Hem). Polished sections, SEM images, BSE mode

This is the peer-reviewed, final accepted version for American Mineralogist, published by the Mineralogical Society of America.
The published version is subject to change. Cite as Authors (Year) Title. American Mineralogist, in press.
DOI: https://doi.org/10.2138/am-2022-8620. http://www.minsocam.org/

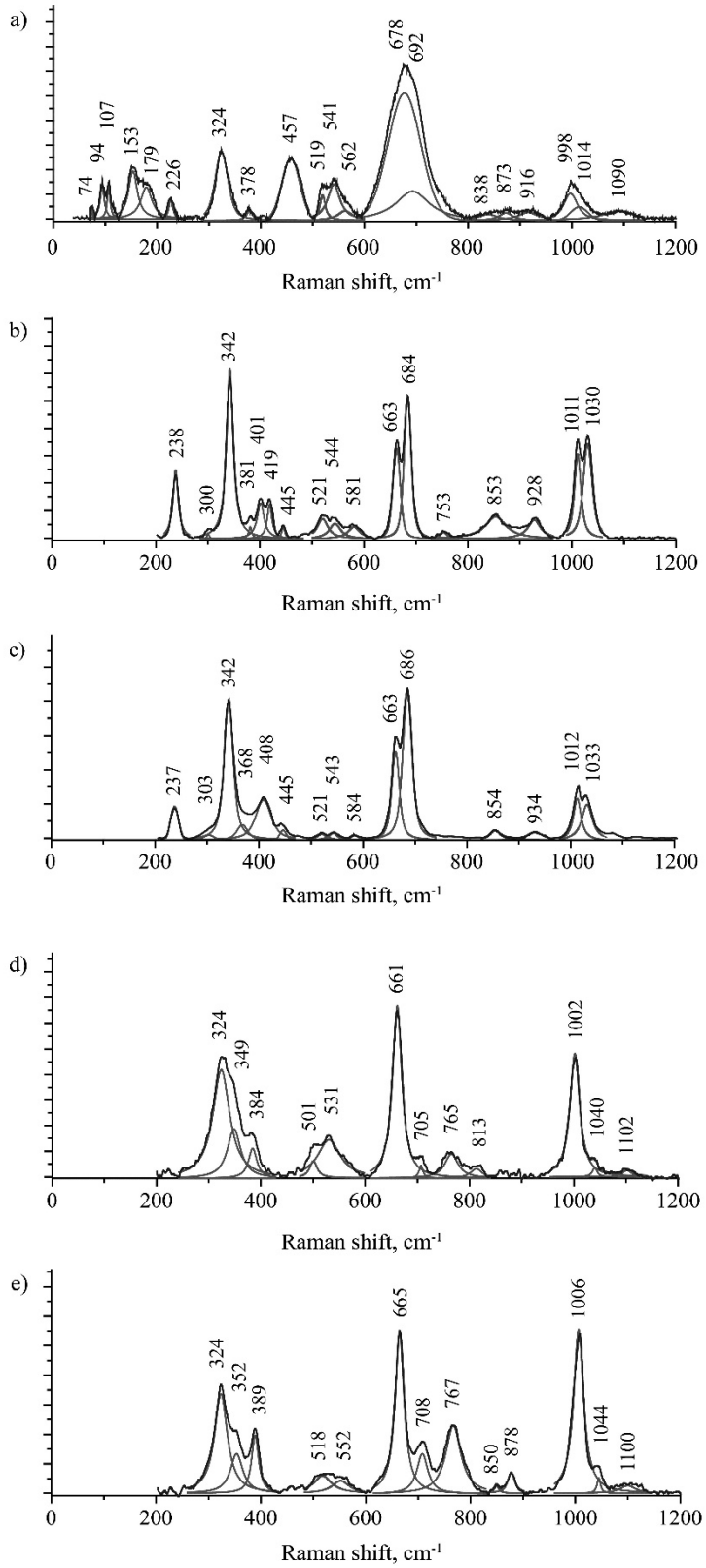

Figure 3 The Raman spectra of ryabchikovite (a), clinoenstatite (sp. gr. $P2_1/c$) (b), enstatite (*Pbca*) (c) and diopside ($C2/c$) (d and e), all from the Arsenatnaya fumarole.

This is the peer-reviewed, final accepted version for American Mineralogist, published by the Mineralogical Society of America.
The published version is subject to change. Cite as Authors (Year) Title. American Mineralogist, in press.
DOI: https://doi.org/10.2138/am-2022-8620. http://www.minsocam.org/

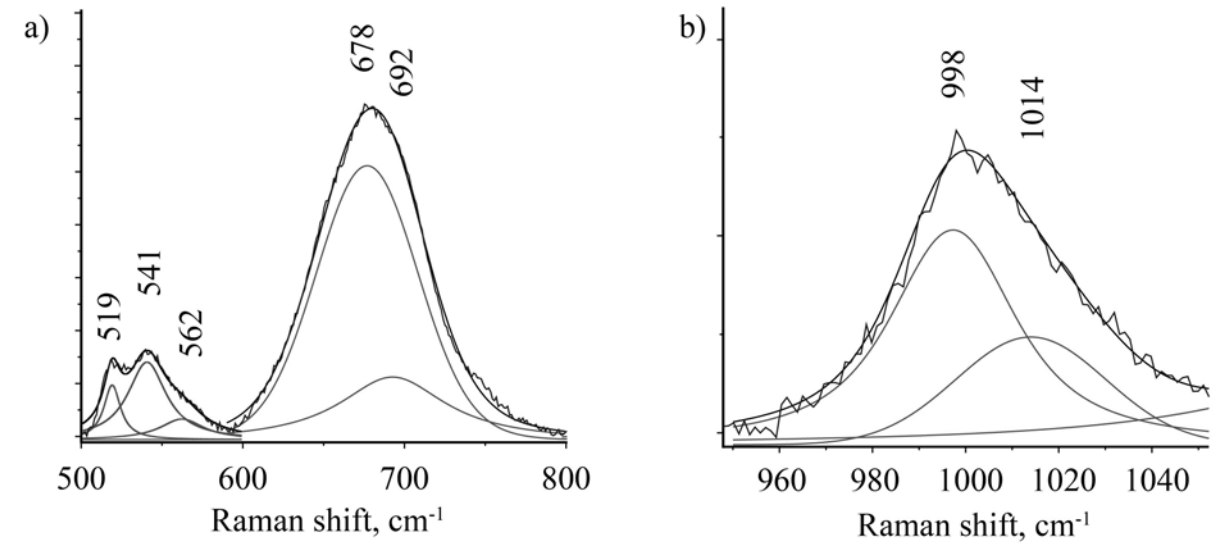

Figure 4. Fragments of the Raman spectrum of ryabchikovite with bands in the regions 500–800 and 930–1080 cm^{-1}.

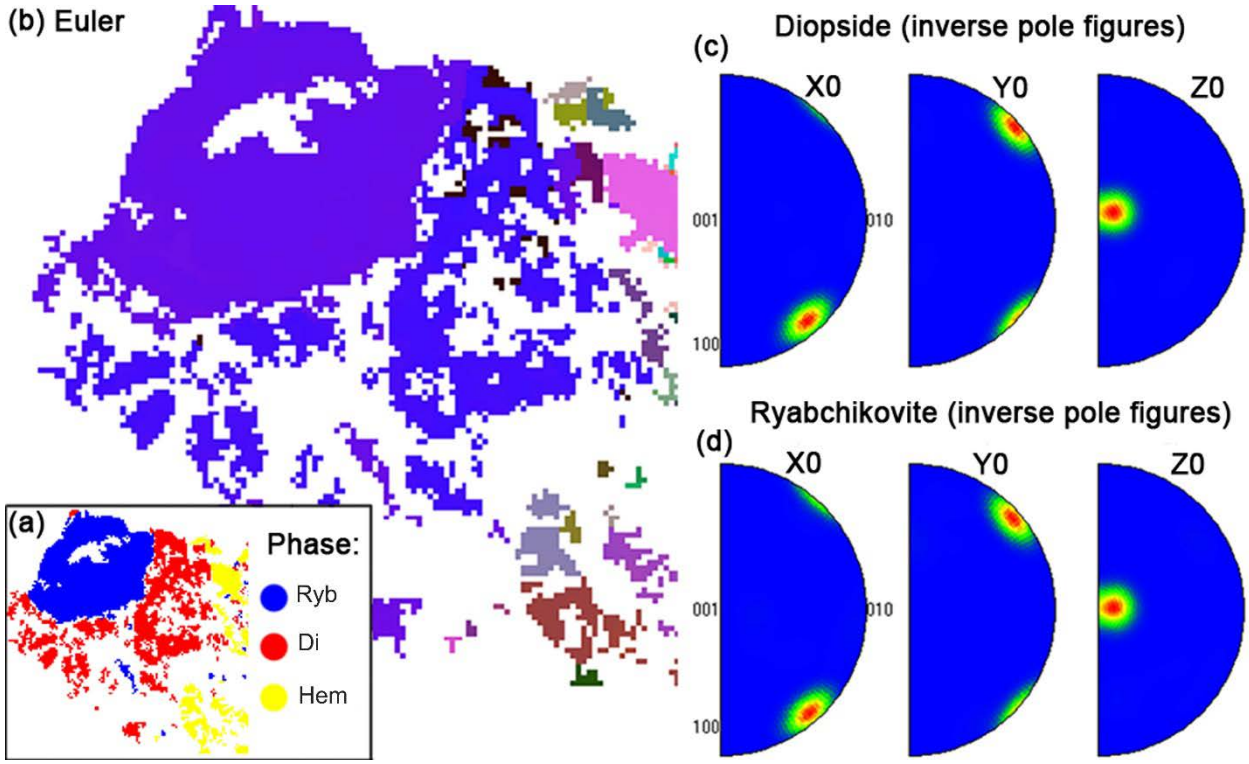

Figure 5. EBSD maps of polished sample with ryabchikovite (Ryb), diopside (Di) and hematite (HEM) from the Arsenatnaya fumarole: (a) mineral distribution map, (b) orientation map, (c) diopside crystals orientation, (d) ryabchikovite crystals orientation.

This is the peer-reviewed, final accepted version for American Mineralogist, published by the Mineralogical Society of America.
The published version is subject to change. Cite as Authors (Year) Title. American Mineralogist, in press.
DOI: https://doi.org/10.2138/am-2022-8620. http://www.minsocam.org/

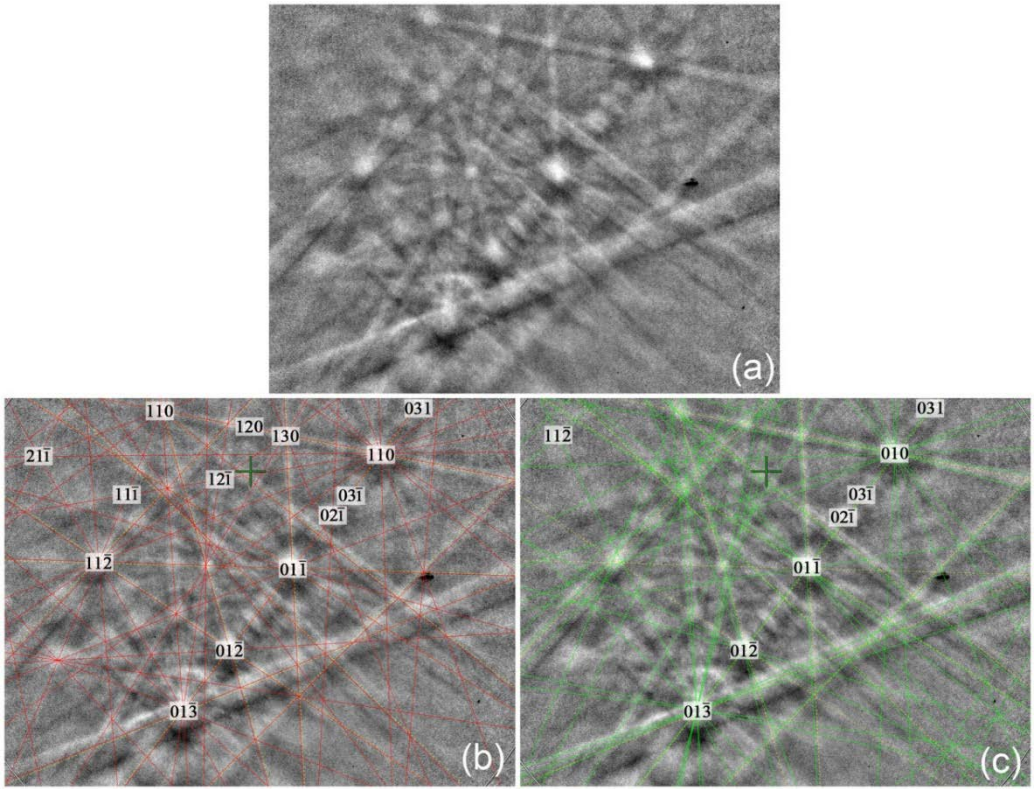

Figure 6. Example of Electron Backscatter Diffraction (EBSD) pattern (a) indexation using theoretical Kikuchi pattern generated from (b) synthetic monoclinic pyroxene $Cu_{0.8}Mg_{1.2}Si_2O_6$ (Ding *et al*., 2016) and (c) synthetic orthorhombic pyroxene $(Cu_{0.56}Mg_{0.44})MgSi_2O_6$ (Tachi *et al*., 1997).

This is the peer-reviewed, final accepted version for American Mineralogist, published by the Mineralogical Society of America.
The published version is subject to change. Cite as Authors (Year) Title. American Mineralogist, in press.
DOI: https://doi.org/10.2138/am-2022-8620. http://www.minsocam.org/

683

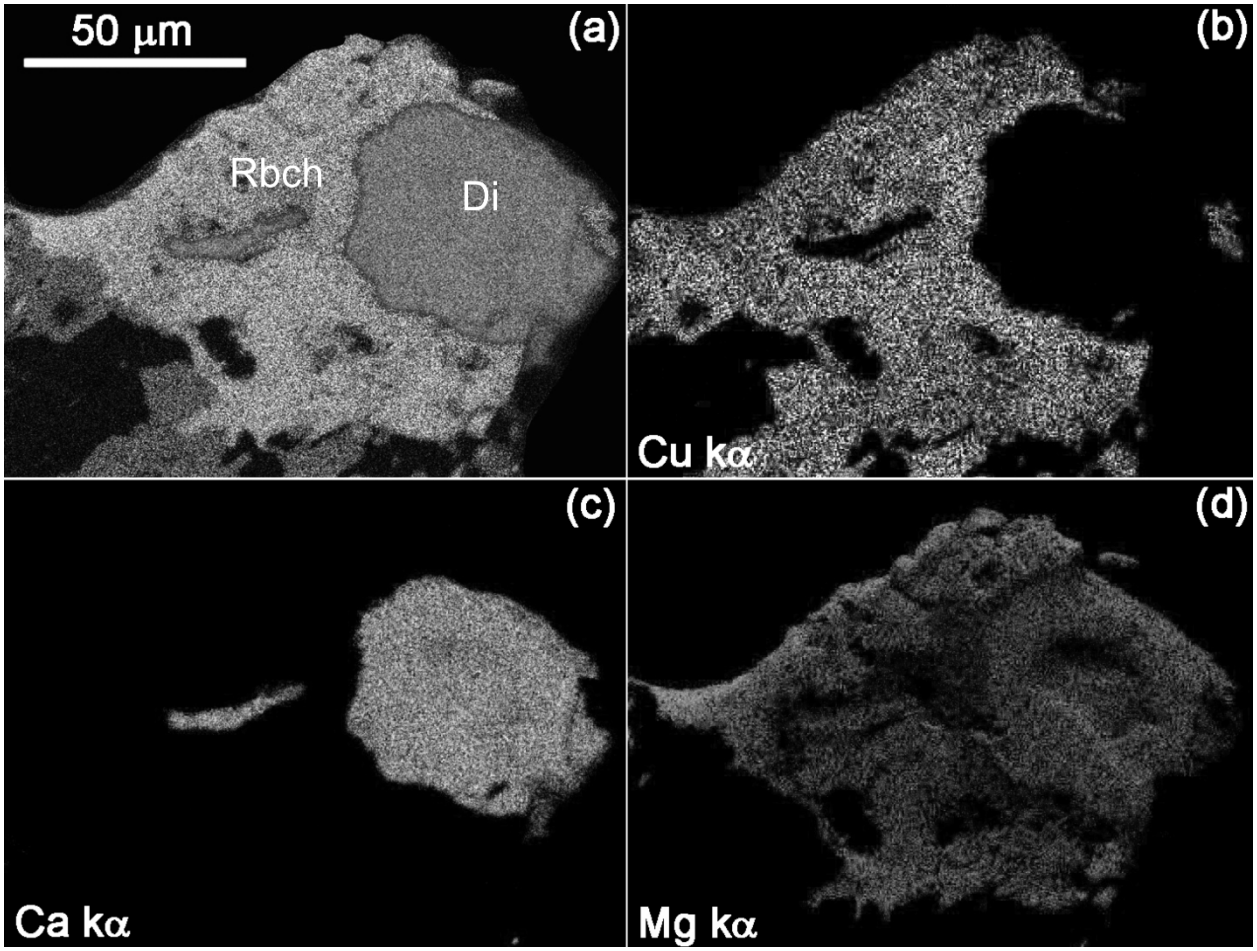

684
685 Figure 7. Elemental maps of diopside (Di) – ryabchikovite (Ryb) intergrowth : (a) Ca-Cu-Mg,
686 (b) CuKα, (c) Ca Kα and (d) Mg Kα.